Cell Reports
Physical Science

CellPress
OPEN ACCESS

Article

Fused aromatic networks with the different spatial arrangement of structural units

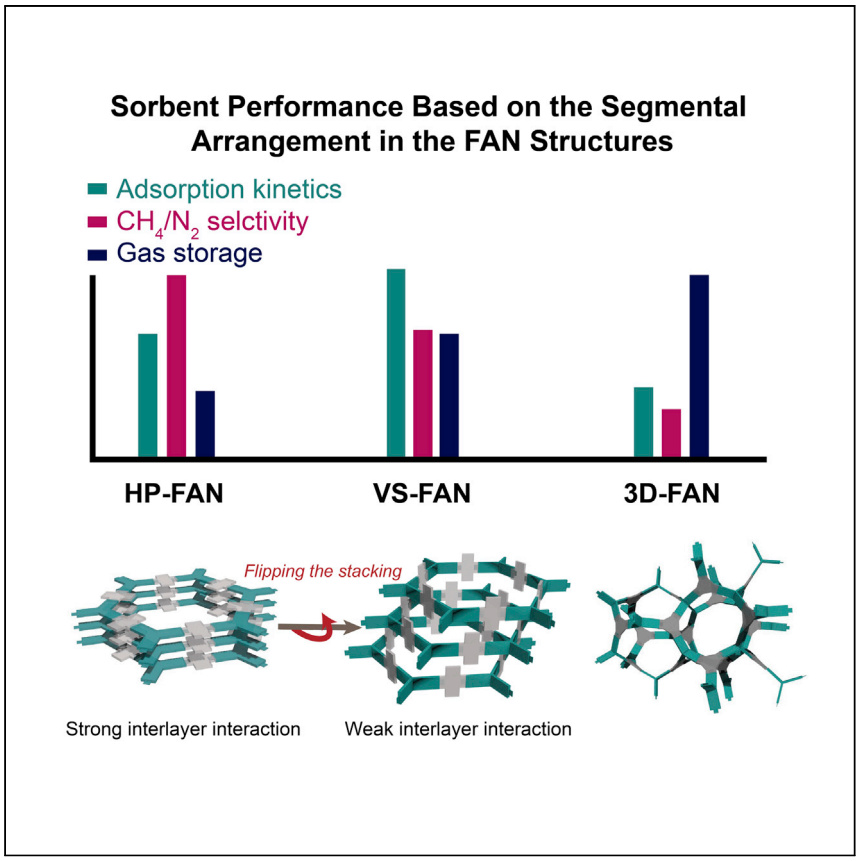

Is there a difference in gas adsorption characteristics depending on the polymer growth direction and the monomer symmetry? Kim et al. design planar 2D, vertically standing 2D, and porous 3D fused aromatic networks (FANs) based on the monomer symmetry and show the gas adsorption and separation properties and their kinetics according to the structures.

Seok-Jin Kim, Tea-Hoon Kim, Ishfaq Ahmad, ..., Javeed Mahmood, Youn-Sang Bae, Jong-Beom Baek

javeed@unist.ac.kr (J.M.)
mowbae@yonsei.ac.kr (Y.-S.B.)
jbbaek@unist.ac.kr (J.-B.B.)

Highlights

FAN structures are vertically, horizontally, and three-dimensionally linked

As sorbent materials, vertically standing FAN has the fastest adsorption kinetics

Horizontally planar FAN has the highest gas separation selectivity

Three-dimensionally arranged FAN shows the highest gas adsorption capacity

Kim et al., Cell Reports Physical Science 2, 100502
July 21, 2021
https://doi.org/10.1016/j.xcrp.2021.100502

Cell Reports
Physical Science

CellPress
OPEN ACCESS

Article

Fused aromatic networks with the different spatial arrangement of structural units

Seok-Jin Kim,[1,3,4] Tea-Hoon Kim,[2,3] Ishfaq Ahmad,[1] Hyuk-Jun Noh,[1] Sun-Min Jung,[1] Yoon-Kwang Im,[1] Javeed Mahmood,[1,*] Youn-Sang Bae,[2,*] and Jong-Beom Baek[1,5,*]

SUMMARY

Fused aromatic networks (FANs) are a new generation of porous organic networks (PONs), which are thermodynamic products. FANs are also kinetic products with low crystallinity. Nevertheless, their high physicochemical stability suggests many potential applications. This work reports three structures with their fully fused aromatic units vertically (V), horizontally (H), and three-dimensionally (3D) linked to the growth direction, forming "standing" FAN (VS-FAN), "planar" FAN (HP-FAN), and 3D-FAN, respectively. Their performance as sorbent materials was evaluated. While the VS-FAN has the fastest kinetics for CH_4 and I_2 adsorption due to the highest segmental freedom, the HP-FAN exhibits the best separation selectivity of the CH_4/N_2 mixture due to the strongest segmental confinement. The 3D-FAN displays the highest adsorption capacity of CH_4 because of the highest specific surface area. The results suggest that the different segmental arrangements may critically affect the sorbent performance of FANs.

INTRODUCTION

In the rapidly expanding field of novel two-dimensional (2D) and 3D network structures, most studies have focused on the synthesis of typical horizontally planar 2D structures such as graphene, boron nitride (BN), metal-organic frameworks (MOFs), and covalent organic frameworks (COFs).[1,2] These materials can be designed and synthesized using a combination of building blocks (monomers) in a logical manner.[3,4] In general, most reported MOFs and COFs are principally composed of coordination or covalent bonds between the building blocks. However, these structures typically have weak linkages formed by reversible reactions, which hinder their practical applications.[5]

Among the strategies for achieving environmental stability for practical applications, considerable attention is being given to the formation of stable linkages formed.[6–11] These include stable fused aromatic networks (FANs) containing fused *N*-heteroacene conjugated backbones, which are advantageous for gas uptake,[12,13] electronics,[14,15] and stabilizing electrocatalysts[16,17] due to the presence of highly polar nitrogen (N) atoms by irreversible reactions.[18,19]

The dimensions and chemical properties of FANs can be controlled by choosing a suitable monomer symmetry and functional groups. However, most designed FAN materials have a conventional "planar" structure, composed of horizontally flat building blocks with interlayer π-π stacking. Strong interlayer attraction leads to the loss of adsorption sites and various properties, which strongly depend on the stacking pattern.[20,21] Many studies have reported efforts to prevent interlayer

[1]School of Energy and Chemical Engineering/Center for Dimension-Controllable Organic Frameworks, Ulsan National Institute of Science and Technology (UNIST), 50 UNIST, Ulsan 44919, Republic of Korea

[2]Department of Chemical and Biomolecular Engineering, Yonsei University, 50 Yonsei-ro, Seodaemun-gu, Seoul 03722, Republic of Korea

[3]These authors contributed equally

[4]Present address: Advanced Membranes & Porous Materials Center and the KAUST Catalysis Center, Physical Science & Engineering, King Abdullah University of Science and Technology (KAUST), Thuwal 23955, Saudi Arabia

[5]Lead contact

*Correspondence: javeed@unist.ac.kr (J.M.), mowbae@yonsei.ac.kr (Y.-S.B.), jbbaek@unist.ac.kr (J.-B.B.)

https://doi.org/10.1016/j.xcrp.2021.100502

interaction, for example, by anchoring bulky and rigid substituents to prevent layer stacking. Still, these methods must sacrifice original structural characteristics.[22–24]

For 3D-FAN structures, suitable molecular building blocks and topologies are limited, mainly due to functional group accessibility, steric hindrance, and kinetic trapping.[25] This issue has also limited the number of attainable 3D structures. Therefore, new building block structures with different connectivity are required, leading to accessible configurations and simplified structural complexity.

To address the aforementioned limitations associated with the structures of horizontally planar (HP)- and 3D-FANs, here, we describe the design and synthesis of a vertically standing (VS) pyrazine-linked network structure, which consists of fully fused aromatic linkages. Due to the vertically linked building units and a high degree of segmental freedom, the vertically standing (VS)-FAN structure can be expected to minimize interlayer π-π stacking while inflating accessible surface areas to provide new diverse topologies beyond the typical HP-FAN and 3D-FAN.[26] In comparison studies with HP-FAN and 3D-FAN, the VS-FANs have higher segmental freedom and a more structurally accessible adsorption area. The VS-FAN exhibits the highest iodine capture rate (1.51 mmol g^{-1} h^{-1}) and uptake capacity (~4.2 g g^{-1}) while displaying intermediate separation performance and gas storage. The separation and adsorption results of CH_4/N_2 fell in between those of the structurally confined HP-FAN and 3D-FAN.

RESULTS

Design of three different types of FAN structures

To investigate structural properties, all of the FAN structures were synthesized by condensation between *o*-diamine and *1,2*-diketone groups containing building blocks in an acidic condition, forming fused aromatic phenazine rings (Figure 1; see Method details). For example, triptycene hexamine (THA) and pyrene-4,5,9,10-tetrone (tetraketopyrene, TKP) were selected as the building blocks to prepare VS-FAN. To compare the effects of structural dimensions, we also prepared a pyrazine-linked HP-FAN and 3D-FAN.[27]

All of the structural units were linked via fused aromatic rings, which impart physicochemical and thermodynamic stability. The structural units of the HP-FAN are connected parallel to the growth direction, but those of VS-FAN are linked vertically to the growth direction. 3D-FAN, which has an arbitrary distributed triptycene unit in 3D space,[27] was also prepared to compare the relationship between the structure and dimension of the FANs.

The structural analyses were conducted using various techniques, including X-ray photoelectron spectroscopy (XPS), elemental analysis (EA), powder X-ray diffraction (XRD), Brunauer-Emmett-Teller (BET) analysis, cross-polarization/magic angle spinning (CP/MAS), ^{13}C nuclear magnetic resonance (^{13}C NMR), scanning electron microscopy (SEM), and high-resolution-transmission electron microscopy (HR-TEM).

The atomic composition and bonding nature of the network structures were confirmed by XPS survey spectra (Table S1), which revealed that samples contained carbon (C), nitrogen (N), and oxygen (O). From the deconvoluted XPS spectra, pyridinic N (398.28 eV), C−N (294.96 eV), and C=O (531.42 eV, related to remnant edge C=O groups) peaks were identified (Figures S1–S3). The EA results were also well matched with the theoretical values (Table S2). In addition, HP-FAN and VS-FAN had an almost identical bonding nature, indicating that they consisted of similar chemical bonds but

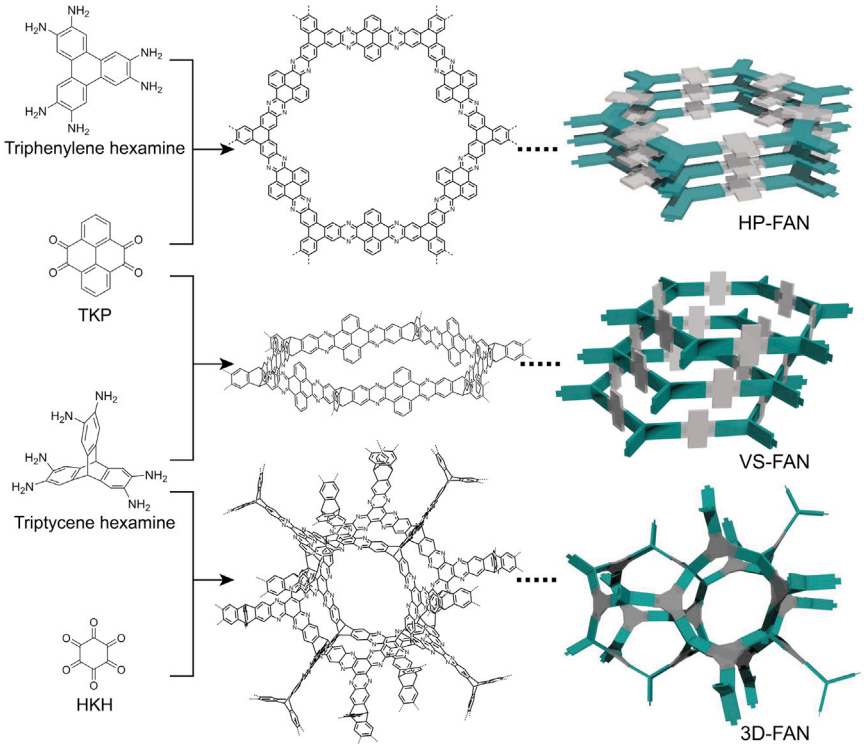

Figure 1. Idealized schematic illustration of 3 FAN structures
Conventional horizontally planar FAN (HP-FAN), vertically standing FAN (VS-FAN), and 3-dimensional FAN (3D-FAN) structures.

different structures. Because they are kinetic products, highly crystalline FAN structures could not be obtained, the XRD pattern could discern the unique structural differences between the three structures. The peak around 26° in the HP-FAN structure corresponded to the interlayer van der Waals distance, while VS-FAN did not show the peak (Figure 2A). This result indirectly indicated that the HP-FAN structure had a strong interlayer π-π interaction between the planes (more close packing), but VS-FAN had a different stacking pattern, with minimal edge-on contact.

The N_2 adsorption/desorption isotherm at 77 K provides information about porosity in relation to the structural geometry (Figure 2B). As expected, 3D-FAN exhibited the highest surface area and total pore volume (1,373.42 $m^2\ g^{-1}$ and 0.64 $cm^3\ g^{-1}$). Interestingly, VS-FAN showed similar results (1,336.22 $m^2\ g^{-1}$ and 0.60 $cm^3\ g^{-1}$) to 3D-FAN. The result suggests that the high surface area is affected by the triptycene units, which induce intrinsic pore volume in the two structures.[28,29] However, the HP-FAN exhibited a relatively lower surface area (743.45 $m^2\ g^{-1}$) and pore volume (0.35 $cm^3\ g^{-1}$) due to its stacking layered nature.

The pore size distribution (PSD), determined using the non-local density functional theory (NLDFT) method, showed the four major pore widths in the three structures centered at ~0.6, 0.8, 1.1, and 1.3 nm, respectively (inset, Figure 2B). Only the 3D-FAN had a slightly smaller pore width of 1.1 nm. Regardless of whether the structure was lying or standing, HP-FAN and VS-FAN revealed similar PSD trends, but HP-FAN had a higher ratio (1.26) of small pores (<1 nm)/large pores (between 1 and 2 nm) than that of VS-FAN (0.85). This means that the layered 2D structure permits a smaller pore width. From the BET analysis, the VS-FAN structure can be

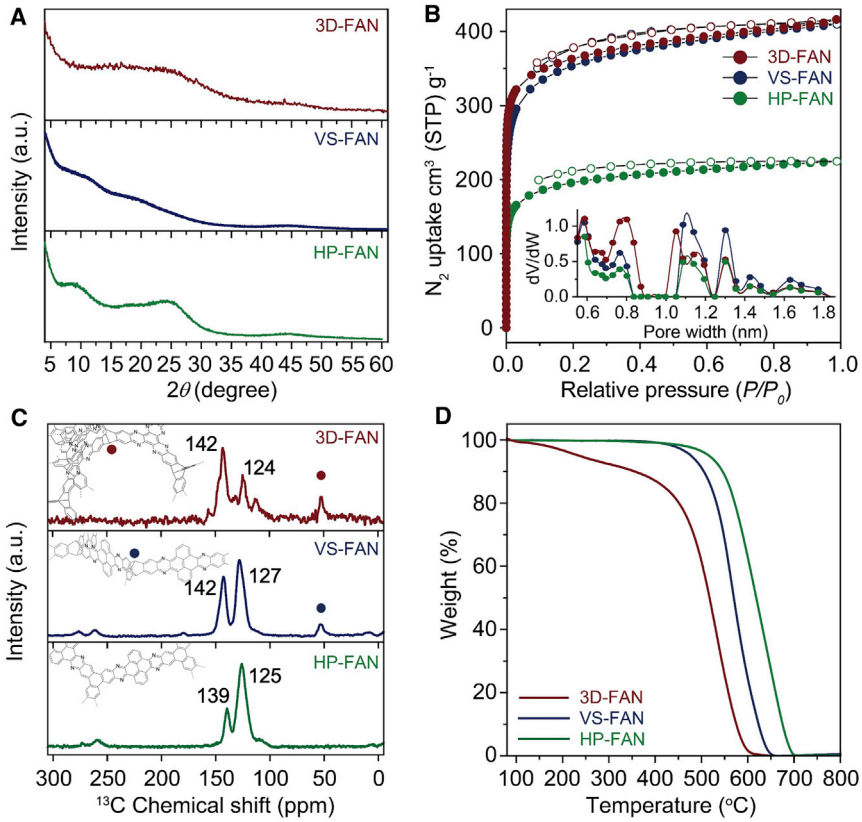

Figure 2. Structural analysis of HP-FAN, VS-FAN, and 3D-FAN

(A) Powder X-ray diffraction patterns.

(B) Nitrogen adsorption/desorption isotherms measured at 77 K. Filled circles, adsorption; blank circles, desorption. Inset: NLDFT pore size distribution for pore width (nm) and dV/dW ($cm^3\ g^{-1}\ nm^{-1}$).

(C) Cross-polarization/magic angle spinning (CP/MAS) ^{13}C NMR spectra.

(D) Thermogravimetric analysis (TGA) curves were obtained with a ramping rate of $10°C\ min^{-1}$ in the air atmosphere.

understood to have minimal π-π stacking, and thus it behaved like the 3D-FAN structure since the adsorbates had more freedom to access pores.

CP/MAS ^{13}C NMR spectroscopy critically confirmed their structural differences (Figure 2C). For HP-FAN, the strong peak at 125 ppm is related to the C in the pyrene and triphenylene moieties, and the peak at 139 ppm is associated with phenazine C (C=N) formed by the reaction of diamine and diketone moieties. Like the HP-FAN structure, the VS-FAN structure also revealed respective peaks at 127 and 142 ppm, which are related to the carbons in the phenyl and phenazine rings. The notable distinction between the two structures was the bridging C in the triptycene moiety in VS-FAN, which appeared at 54 ppm (the dark blue dot in Figure 2C).[27,30] In the 3D-FAN spectrum, there were minor peaks around the pyrazine bond, due to the relatively large number of edges, and a slightly different chemical environment as it divergently grew into 3D space.[27]

The SEM images of HP-FAN (Figure S4), VS-FAN (Figure S5), and 3D-FAN (Figure S6) show a corrugated surface morphology. However, obtaining informative TEM images was difficult for all of the samples due to the rapid beam damage (Figures S7–S9).[30]

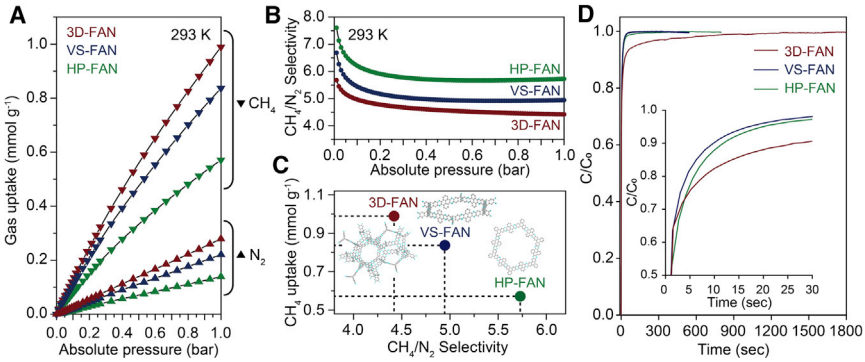

Figure 3. CH_4 and N_2 gas adsorption properties of HP-FAN, VS-FAN, and 3D-FAN

(A) Adsorption amount (mmol g^{-1}) of CH_4 (downward triangle) and N_2 (upward triangle).

(B) Separation selectivity of IAST-predicted CH_4/N_2 mixture at 293 K.

(C) CH_4 uptake capacities and selectivity trends extracted from (A) and (B).

(D) Time-dependent CH_4 kinetic uptake profiles at 293 K and 0.5 bar (C/C_0: fractional uptake).

The 2D network structures showed higher thermal stability than the 3D-FAN in the thermogravimetric analysis (TGA) (Figure 2D) because the 3D structure had more dangling edges. Among the FAN structures, HP-FAN showed better thermal stability than VS-FAN due to its layered nature and efficiently packed structure.

Methane adsorption and separation

To investigate the relationship between structure and gas uptake property, CH_4 and N_2 adsorption studies were conducted (Figures 3 and S10). The amounts of CH_4 adsorbed under 1 bar at 293 K were 0.57 mmol g^{-1} for HP-FAN, 0.84 mmol g^{-1} for VS-FAN, and 0.99 mmol g^{-1} for 3D-FAN (Figure 3A). N_2 uptakes were found to be 0.14 mmol g^{-1}, 0.22 mmol g^{-1}, and 0.28 mmol g^{-1}, respectively. The trend in gas uptake increased from the flat 2D to standing 2D to a 3D structure. In addition, the results for low- and high-pressure isotherms at 298 K showed similar trends (Figure S11). The CH_4 adsorption was higher overall than N_2 because there was a more effective interaction between the CH_4 and polar bonds such as C–N due to its slightly larger polarizability.[31]

Based on the results of CH_4/N_2 adsorption, the samples were subjected to a challenge, the separation of methane (CH_4) and nitrogen (N_2), because of the similarity in physicochemical properties, especially their kinetic diameters (CH_4: 3.80 Å and N_2: 3.64 Å).[32,33] The selectivity was fitted using the dual-site Langmuir-Freundlich isotherm model.[34] High selectivity is required for separation systems in natural gas refining. The ideal adsorbed solution theory (IAST)-predicted CH_4/N_2 (50:50) selectivity, indicating 5.73, 4.95, and 4.42 for HP-FAN, VS-FAN, and 3D-FAN, respectively (Figure 3B; Table S3).[35] Combining the preceding results, Figure 3C shows the relationship between CH_4 uptake (HP-FAN < VS-FAN < 3D-FAN) and selectivity (HP-FAN > VS-FAN > 3D-FAN).

Although IAST-predicted selectivity has been widely used for gas separation, it does not provide real gas characteristics such as kinetics and dynamic flow. To investigate the effect of differences in structural dimensions on CH_4/N_2 separation performance under dynamic mixture flow, breakthrough experiments were performed at 298 K using packed beds containing 3 different materials (Figure S12). From the results of binary-component separation, the selectivities of HP-FAN, VS-FAN, and 3D-FAN were on the order of 2.48, 2.16, and 1.92, showing a similar tendency to selectivity

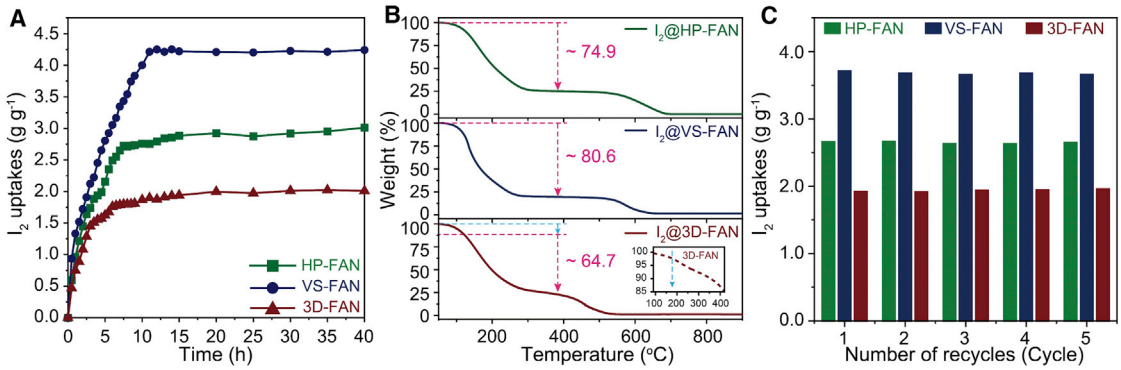

Figure 4. Iodine adsorption behaviors of HP-FAN, VS-FAN, and 3D-FAN

(A) Gravimetric I_2 uptake capacity at 350 K with respect to time.

(B) TGA thermograms of I_2 adsorbed structures under air condition (inset: TGA curve of pristine 3D-FAN before I_2 adsorption measured in the air).

(C) Recyclability of the I_2 capture properties.

calculated by IAST. Three consecutive repeated breakthrough experiments displayed practically applicable stability, as all of the FAN structures maintained a similar separation performance.

To further investigate the advantages of VS-FAN, the kinetic absorption curves of CH_4 were obtained at 293 K (Figure 3D). The CH_4 diffusivities were calculated using a classical micropore diffusion model (Table S4). Unlike the typical adsorption and separation trends of 2D layered and porous 3D materials, the VS-FAN exhibited the fastest uptake kinetics. Based on this result, the advantages of VS structure can minimize interlayer interactions, and thus maximize segmental motion compared to typical layered planar 2D and porous 3D structures, allowing gas molecules to reach the adsorption surface in a short time. Thus, the VS-FAN has substantial kinetic advantages for specific applications over conventional sorbent materials.

Iodine adsorption

In addition, rapid adsorption is an essential factor for removing harmful gases at a minimum exposure time. The VS-FAN structure can be a suitable candidate for adsorbing harmful gases due to its fastest diffusivity and accessibility, which are accelerated by the maximum exposure of electron-localized pyrazine N atoms in the structure. To investigate the efficiency of FANs with respect to structure and dimensionality, we carried out iodine (I_2: 3.35 Å) capture (Figure 4). Phenazine-bridged microporous polymers have shown a high capacity for radioactive I_2 capture due to their effective adsorption sites, such as electron-rich N atoms and a π-electron conjugated structure.[36,37] Based on the reported I_2 capture performance of porous organic networks,[26,36,38,39] HP-FAN and VS-FAN were expected to show good I_2 uptake properties (see also Table S6). This is because the electron-deficient I_2 prefers a lone pair electron in pyrazine N as well as a π-electron cloud of pyrene units.

The VS-FAN was found to have the highest I_2 adsorption value of ~4.2 g g^{-1} (Figure 4A). Compared with HP-FAN (~3.0 g g^{-1}), VS-FAN exhibited higher I_2 capture. This performance is associated with a higher surface area and segmental freedom due to the weaker interlayer interaction. Although those two samples were structurally similar, the HP-FAN structure sacrifices adsorption sites due to the π-π stacking. The 3D-FAN showed the lowest I_2 uptake (~2.0 g g^{-1}) due to the absence of pyrene units. It had a relatively smaller π-conjugated aromatic area than HP-FAN and VS-FAN, indicating that triptycene units do not significantly contribute to I_2 uptake.

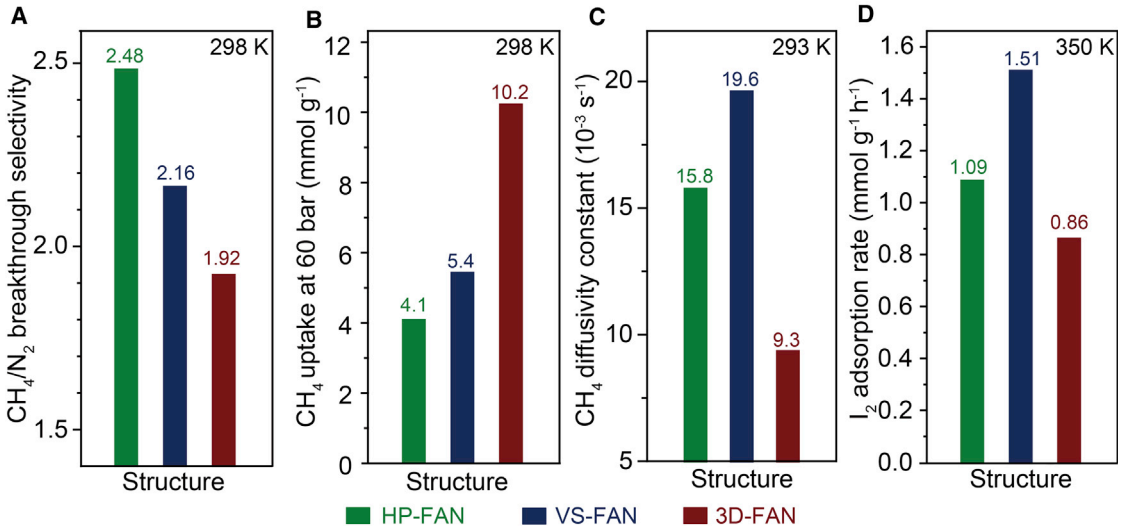

Figure 5. Adsorption behaviors of HP-FAN, VS-FAN, and 3D-FAN

(A) CH_4/N_2 breakthrough selectivity.

(B) Amount of CH_4 adsorption at 60 bar.

(C) CH_4 diffusivities at 293 K.

(D) Rate of iodine adsorption at 350 K.

The adsorption amounts were re-confirmed using TGA measurements (Figure 4B). The 3D-FAN was calculated by considering moisture and mass reduction due to the dissipation of the terminal groups up to 400°C (~14%; sky blue arrow in the inset of Figure 4B; see also Figure 2D) before the I_2 adsorption test. In addition, XPS spectra support that I_2 is adsorbed in the pores of FANs (Figure S13).

The recyclability tests were conducted after repeatedly washing with ethanol. The 3D-FAN showed an adsorption reproducibility of ~95% after the first cycle, but the other FAN structures remained at 86%–88% after the first cycle (Figure 4C). This is probably because the I_2 that was first adsorbed was not thoroughly washed off with ethanol because of the strong interaction between I_2 and the structures. Except for the first cycle, all of the structures exhibited stable adsorption performance from the second to the fifth cycles.

Relationship between FAN structures and adsorption behaviors

The adsorption and separation characteristics of the FANs can be clearly distinguished depending on structure and dimensionality (Figure 5; Tables S4 and S5). Regarding gas separation, the HP-FAN showed excellent performance due to the confined layered structure and the high ratio of small/large pore sizes. The VS-FAN had intermediate selectivity between the HP-FAN and porous 3D-FAN (Figure 5A).

The tendency for gas storage performance was the opposite of that for separation (Figure 5B). The adsorption amount gradually increased with dimensionality, from flat 2D to standing 2D to 3D structures. This is because adsorption space is lost due to strong interlayer interactions in the HP-FAN structure. In the case of 3D-FAN, the adsorption spaces are all open so that the gases can freely access the structure. Although the VS-FAN had a completely open surface, like the 3D-FAN, the uptake capacity was relatively lower because a little π-π interaction may still have existed in the collapsed area.

Although the VS-FAN showed an intermediate performance in adsorption and separation between the conventional flat 2D and porous 3D structures, it has the highest gas diffusivity constant (Figure 5C). There must be a possibility to overcome limiting factors in capturing reaction intermediate and enhancing separation selectivity because the VS-FAN has a kinetic advantage.

Along with uptake capacity, rapid adsorption is significant to remove harmful substances, such as radiative I_2. From a kinetic perspective, the VS-FAN showed outstanding performance for the I_2 uptake rate (Figure 5D). These results were associated with good accessibility to the aromatic adsorption sites due to high segmental flexibility. This indicates that VS-FAN had fewer π-π interactions from the perpendicularly connected structural units, resulting in loose packing with minimal edge-on contact, which in turn yielded more accessible pores and free volume.[40] Although the HP-FAN structure had similar aromatic structural units to the VS-FAN, accessible space was reduced by the interlayer stacking. The 3D-FAN had a larger surface area, but there was a kinetic delay before the bulky I_2 molecules reached the inner pores. Therefore, the VS-FAN structure was determined to have an advantage over the HP-FAN and 3D-FAN structures from a kinetic perspective.

DISCUSSION

Three different FAN structures were designed and synthesized with different structures and dimensionality. A comparative study of the gas sorption and separation behaviors of the pyrazine-linked FANs found that the porous 3D-FAN had the best gas uptake capacity because of its intrinsic microporous channels, and the HP-FAN demonstrated the best CH_4/N_2 separation performance due to its confined layered nature. The VS-FAN displayed intermediate gas uptake and separation performance compared with the HP-FAN and 3D-FAN structures. However, because of the highly available extended π-conjugated surface area and degree of segmental freedom, VS-FAN exhibited the best kinetic diffusivity and I_2 uptake performance. Thus, the results presented in this study suggest that the segmental arrangement of FAN materials is crucial for specifically different applications such as harmful gas adsorption, rapid sensing, and fast catalytic reaction. Furthermore, this study is expected to be helpful in the design of more unique porous crystalline materials such as COFs or MOFs. It is anticipated that standing-type structures can be applied to gas adsorption applications more efficiently and with high performance if a synthetic strategy is conceived to form crystalline standing structures.

EXPERIMENTAL PROCEDURES

Resource availability

Lead contact

Further requests for resources and reagents should be directed to and will be fulfilled by the lead contact, Jong-Beom Baek (jbbaek@unist.ac.kr).

Materials availability

Commercially available reagents were used without further purification. Solvents were purified before use according to the standard procedures. All of the reactions were conducted under inert conditions unless otherwise stated.

Data and code availability

The authors declare that supporting data and the findings of this study are available within the article and the Supplemental information. All other data are available from the lead contact upon reasonable request.

Synthesis of HP-FAN

Triphenylene-2,3,6,7,10,11-hexamine hexahydrochloride (1.5 g, 2.79 mmol), dihydropyrene-4,5,9,10-tetraone (1.09 g, 4.18 mmol) trifluoromethanesulfonic acid (TFMSA) (40 mL) were charged into a 3-neck round-bottomed flask (250 mL) in an ice bath. The mixture was slowly warmed up to room temperature for 12 h and then heated to 175°C for 3 h. After 1 h, the thin liquid was converted into a gel-like mixture. The temperature was maintained for an additional 2 h to ensure complete reaction and then cooled down to room temperature. The gel-like product was precipitated in deionized water, collected by filtration on a polytetrafluoroethylene (PTFE) membrane (0.45 μm pore size), and repeatedly washed with water. The product was further Soxhlet extracted with water and MeOH for 3 days each and freeze-dried at −120°C under reduced pressure (0.05 mm Hg) for 3 days (see also Supplemental experimental procedures).

Synthesis of VS-FAN

In a 3-neck round-bottomed flask (250 mL), THA hexahydrochloride (1.0 g, 1.7 mmol) and dihydropyrene-4,5,9,10-tetraone (0.70 g, 2.67 mmol) were charged in freshly distilled TFMSA (35 mL) in an ice bath. After stirring at 0°C for 1 h, the ice bath was replaced with an oil bath and the temperature gradually increased to 175°C. The rest of the workup procedure was similar to the HP-FAN.

Synthesis of 3D-FAN

Following the literature procedure,[27] triptycene hexamine hexahydrochloride (0.5 g, 0.88 mmol), hexaketocyclohexane (HKH) octahydrate (0.277 g, 0.88 mmol), and TFMSA (40 mL) were charged into a 3-neck round-bottomed flask (250 mL) in an ice bath. The mixture was slowly warmed to room temperature for 12 h and then heated to 175°C for 3 h. The rest of the workup procedure was similar to that of the HP-FAN.

Breakthrough experiment

Samples were initially activated at 150°C for 3 h under a high vacuum before packing the column. Each activated sample, HP-FAN (0.4280 g), VS-FAN (0.4277 g), and 3D-FAN (0.3184 g), was packed into a stainless-steel column ($^1/_4$ in × 150 mm). The length of each sample occupied in the column was 44, 50, and 74 mm, respectively. The rest of the column was filled with glass beads (750 μm), and each layer used glass wool. Before the breakthrough test, the packed column was degassed with a helium (He) flow of 46 mL min^{-1} at 150°C for 1 h in the breakthrough system. The experiment was carried out at a total flow rate of 5 mL min^{-1} with a binary feed gas mixture (CH_4/N_2, 50:50 vol%) at 25°C, 1 atm. After the separation was completed, the sample was mildly regenerated (He 5 mL min^{-1}, 6 min) without increasing the temperature, and the same procedure was repeated 3 times for reproducibility testing.

Isotherms of iodine adsorption test

All of the samples were vacuum dried at 80°C overnight, and then each sample (60 mg) was placed into a sealed vessel (250 mL) in the presence of excess iodine (700 mg) at 350 K. The adsorption of iodine vapor was directly evaluated by weighing the samples. For crosschecking, the iodine adsorbed samples were also subjected to TGA. During iodine uptake, gravity measurements were performed at different time intervals (measured at intervals of 30 min, 1 h, and 5 h, respectively, based on 9 h, 15 h, and 40 h). The recyclability procedure was carried out after washing with ethanol several times (a total of 10 min), and the process mentioned above was repeated.

SUPPLEMENTAL INFORMATION

Supplemental information can be found online at https://doi.org/10.1016/j.xcrp.2021.100502.

ACKNOWLEDGMENTS

This research was supported by the Creative Research Initiative (CRI, 2014R1A2069102), BK21 Plus (10Z20130011057), the Science Research Center (SRC, 2016R1A5A1009405), the Next Generation Carbon Upcycling Project (2017M1A2A2043449), and Young Researcher Programs (2019R1C1C1006650) through the National Research Foundation (NRF) of Korea.

AUTHOR CONTRIBUTIONS

S.-J.K., J.M., and I.A. prepared materials, and S.-J.K. analyzed structures. T.-H.K. and Y.-S.B. analyzed gas adsorption properties and carried out breakthrough experiments. S.-J.K. and H.-J.N. tested the iodine capture experiments. Y.-K.I. measured the SEM and S.-M.J. took TEM images of the materials. S.-J.K., J.M., and J.-B.B. wrote the manuscript, and all of the authors interpreted the results and commented on the paper.

DECLARATION OF INTERESTS

The authors declare no competing interests.

Received: March 23, 2021
Revised: May 10, 2021
Accepted: June 18, 2021
Published: July 14, 2021

REFERENCES

1. Zeng, M., Xiao, Y., Liu, J., Yang, K., and Fu, L. (2018). Exploring Two-Dimensional Materials toward the Next-Generation Circuits: From Monomer Design to Assembly Control. Chem. Rev. *118*, 6236–6296.

2. Lohse, M.S., and Bein, T. (2018). Covalent Organic Frameworks: Structures, Synthesis, and Applications. Adv. Funct. Mater. *28*, 1705553.

3. Geng, K., He, T., Liu, R., Dalapati, S., Tan, K.T., Li, Z., Tao, S., Gong, Y., Jiang, Q., and Jiang, D. (2020). Covalent Organic Frameworks: Design, Synthesis, and Functions. Chem. Rev. *120*, 8814–8933.

4. Colson, J.W., and Dichtel, W.R. (2013). Rationally synthesized two-dimensional polymers. Nat. Chem. *5*, 453–465.

5. Wu, H.B., and Lou, X.W.D. (2017). Metal-organic frameworks and their derived materials for electrochemical energy storage and conversion: promises and challenges. Sci. Adv. *3*, eaap9252.

6. Zhang, S., Yang, Q., Wang, C., Luo, X., Kim, J., Wang, Z., and Yamauchi, Y. (2018). Porous Organic Frameworks: Advanced Materials in Analytical Chemistry. Adv. Sci. (Weinh.) *5*, 1801116.

7. Das, S., Heasman, P., Ben, T., and Qiu, S. (2017). Porous Organic Materials: Strategic Design and Structure-Function Correlation. Chem. Rev. *117*, 1515–1563.

8. Yuan, Y., and Zhu, G. (2019). Porous Aromatic Frameworks as a Platform for Multifunctional Applications. ACS Cent. Sci. *5*, 409–418.

9. Bildirir, H., Gregoriou, V.G., Avgeropoulos, A., Scherf, U., and Chochos, C.L. (2017). Porous organic polymers as emerging new materials for organic photovoltaic applications: current status and future challenges. Mater. Horiz. *4*, 546–556.

10. Zhang, T., Xing, G., Chen, W., and Chen, L. (2020). Porous organic polymers: a promising platform for efficient photocatalysis. Mater. Chem. Front. *4*, 332–353.

11. Ahmad, I., Mahmood, J., and Baek, J.B. (2020). Recent Progress in Porous Fused Aromatic Networks and Their Applications. Small Sci. *1*, 2000007.

12. Hu, B.L., An, C., Wagner, M., Ivanova, G., Ivanova, A., and Baumgarten, M. (2019). Three-Dimensional Pyrene-Fused N-Heteroacenes. J. Am. Chem. Soc. *141*, 5130–5134.

13. Shin, S.H., Noh, H.J., Kim, Y.H., Im, Y.K., Mahmood, J., and Baek, J.B. (2019). Forming layered conjugated porous BBL structures. Polym. Chem. *10*, 4185–4193.

14. Mahmood, J., Lee, E.K., Jung, M., Shin, D., Jeon, I.Y., Jung, S.M., Choi, H.J., Seo, J.M., Bae, S.Y., Sohn, S.D., et al. (2015). Nitrogenated holey two-dimensional structures. Nat. Commun. *6*, 6486.

15. Li, J.L., Chai, Y.F., Wang, W.V., Shi, Z.F., Xu, Z.G., and Zhang, H.L. (2017). Pyrazine-fused isoindigo: a new building block for polymer solar cells with high open circuit voltage. Chem. Commun. (Camb.) *53*, 5882–5885.

16. Kim, S.J., Mahmood, J., Kim, C., Han, G.F., Kim, S.W., Jung, S.M., Zhu, G., De Yoreo, J.J., Kim, G., and Baek, J.B. (2018). Defect-Free Encapsulation of Fe^0 in 2D Fused Organic Networks as a Durable Oxygen Reduction Electrocatalyst. J. Am. Chem. Soc. *140*, 1737–1742.

17. Mahmood, J., Li, F., Jung, S.M., Okyay, M.S., Ahmad, I., Kim, S.J., Park, N., Jeong, H.Y., and Baek, J.B. (2017). An efficient and pH-universal ruthenium-based catalyst for the hydrogen evolution reaction. Nat. Nanotechnol. *12*, 441–446.

18. Liu, W., Jiang, S.D., Yan, Y., Wang, W., Li, J., Leng, K., Japip, S., Liu, J., Xu, H., Liu, Y., et al. (2020). A solution-processable and ultra-permeable conjugated microporous thermoset for selective hydrogen separation. Nat. Commun. *11*, 1633.

19. Mahmood, J., Anjum, M.A.R., and Baek, J.B. (2019). Fused Aromatic Network Structures as a Platform for Efficient Electrocatalysis. Adv. Mater. *31*, e1805062.

20. Wang, Z., Zhang, S., Chen, Y., Zhang, Z., and Ma, S. (2020). Covalent organic frameworks for separation applications. Chem. Soc. Rev. *49*, 708–735.

21. Wu, X., Han, X., Liu, Y., Liu, Y., and Cui, Y. (2018). Control Interlayer Stacking and Chemical Stability of Two-Dimensional Covalent Organic Frameworks via Steric Tuning. J. Am. Chem. Soc. *140*, 16124–16133.

22. Marco, A.B., Cortizo-Lacalle, D., Perez-Miqueo, I., Valenti, G., Boni, A., Plas, J., Strutyński, K., De Feyter, S., Paolucci, F., Montes, M., et al. (2017). Twisted Aromatic Frameworks: Readily Exfoliable and Solution-Processable Two-Dimensional Conjugated Microporous Polymers. Angew. Chem. Int. Ed. Engl. *56*, 6946–6951.

23. Khayum, M.A., Kandambeth, S., Mitra, S., Nair, S.B., Das, A., Nagane, S.S., Mukherjee, R., and Banerjee, R. (2016). Chemically Delaminated Free-Standing Ultrathin Covalent Organic Nanosheets. Angew. Chem. Int. Ed. Engl. *55*, 15604–15608.

24. Mitra, S., Kandambeth, S., Biswal, B.P., Khayum M, A., Choudhury, C.K., Mehta, M., Kaur, G., Banerjee, S., Prabhune, A., Verma, S., et al. (2016). Self-Exfoliated Guanidinium-Based Ionic Covalent Organic Nanosheets (iCONs). J. Am. Chem. Soc. *138*, 2823–2828.

25. Ma, X.J., and Scott, T.F. (2018). Approaches and challenges in the synthesis of three-dimensional covalent-organic frameworks. Commun. Chem. *1*, 98.

26. Noh, H.J., Im, Y.K., Yu, S.Y., Seo, J.M., Mahmood, J., Yildirim, T., and Baek, J.B. (2020). Vertical two-dimensional layered fused aromatic ladder structure. Nat. Commun. *11*, 2021.

27. Mahmood, J., Kim, S.J., Noh, H.J., Jung, S.M., Ahmad, I., Li, F., Seo, J.M., and Baek, J.B. (2018). A Robust 3D Cage-like Ultramicroporous Network Structure with High Gas-Uptake Capacity. Angew. Chem. Int. Ed. Engl. *57*, 3415–3420.

28. Ghanem, B.S., Msayib, K.J., McKeown, N.B., Harris, K.D.M., Pan, Z., Budd, P.M., Butler, A., Selbie, J., Book, D., and Walton, A. (2007). A triptycene-based polymer of intrinsic microposity that displays enhanced surface area and hydrogen adsorption. Chem. Commun. (Camb.) (1), 67–69.

29. Ghanem, B.S., Hashem, M., Harris, K.D.M., Msayib, K.J., Xu, M.C., Budd, P.M., Chaukura, N., Book, D., Tedds, S., Walton, A., et al. (2010). Triptycene-Based Polymers of Intrinsic Microporosity: Organic Materials That Can Be Tailored for Gas Adsorption. Macromolecules *43*, 5287–5294.

30. Bhola, R., Payamyar, P., Murray, D.J., Kumar, B., Teator, A.J., Schmidt, M.U., Hammer, S.M., Saha, A., Sakamoto, J., Schlüter, A.D., and King, B.T. (2013). A two-dimensional polymer from the anthracene dimer and triptycene motifs. J. Am. Chem. Soc. *135*, 14134–14141.

31. Niu, Z., Cui, X., Pham, T., Lan, P.C., Xing, H., Forrest, K.A., Wojtas, L., Space, B., and Ma, S. (2019). A Metal-Organic Framework Based Methane Nano-trap for the Capture of Coal-Mine Methane. Angew. Chem. Int. Ed. Engl. *58*, 10138–10141.

32. Baker, R.W., and Lokhandwala, K. (2008). Natural gas processing with membranes: an overview. Ind. Eng. Chem. Res. *47*, 2109–2121.

33. Bhadra, S.J., and Farooq, S. (2011). Separation of Methane-Nitrogen Mixture by Pressure Swing Adsorption for Natural Gas Upgrading. Ind. Eng. Chem. Res. *50*, 14030–14045.

34. Yang, R.T. (2003). Adsorbents: Fundamentals and Applications (John Wiley & Sons).

35. Myers, A.L., and Prausnitz, J.M. (1965). Thermodynamics of Mixed-Gas Adsorption. AIChE J. *11*, 121–127.

36. Xie, W., Cui, D., Zhang, S.R., Xu, Y.H., and Jiang, D.L. (2019). Iodine capture in porous organic polymers and metal-organic frameworks materials. Mater. Horiz. *6*, 1571–1595.

37. Tang, Y.Z., Huang, H.L., Li, J., Xue, W.J., and Zhong, C.L. (2019). IL-induced formation of dynamic complex iodide anions in IL@MOF composites for efficient iodine capture. J. Mater. Chem. A Mater. Energy Sustain. *7*, 18324–18329.

38. Pei, C.Y., Ben, T., Xu, S.X., and Qiu, S.L. (2014). Ultrahigh iodine adsorption in porous organic frameworks. J. Mater. Chem. A Mater. Energy Sustain. *2*, 7179–7187.

39. Wang, P., Xu, Q., Li, Z., Jiang, W., Jiang, Q., and Jiang, D. (2018). Exceptional Iodine Capture in 2D Covalent Organic Frameworks. Adv. Mater. *30*, e1801991.

40. Rose, I., Bezzu, C.G., Carta, M., Comesaña-Gándara, B., Lasseuguette, E., Ferrari, M.C., Bernardo, P., Clarizia, G., Fuoco, A., Jansen, J.C., et al. (2017). Polymer ultrapermeability from the inefficient packing of 2D chains. Nat. Mater. *16*, 932–937.